Available online at www.sciencedirect.com
SCIENCE DIRECT®
Earth and Planetary Science Letters 243 (2006) 1 – 14
EPSL
www.elsevier.com/locate/epsl

Lateral variations of lunar crustal thickness from the Apollo seismic data set

H. Chenet [a,*,1], Ph. Lognonné [b], M. Wieczorek [b], H. Mizutani [a,2]

[a] *Planet. Sci. Div., Institute of Space and Astronautical Science, Japan Aerospace eXploration Agency, Yoshinodai 3-1-1, Sagamihara, 229-8510, Japan*

[b] *Etudes Spatiales et Planétologie, Institut de Physique du Globe de Paris, (UMR 7154-CNRS-Université Paris 7), 4 av. Neptune, 94107 Saint-Maur, France*

Received 12 July 2005; received in revised form 14 December 2005; accepted 16 December 2005
Available online 3 February 2006
Editor: S. King

Abstract

Seismic waves generated by meteoroid impacts have been detected by the Apollo lunar seismic network. These waves are sensitive to the crustal structure beneath both the seismic stations and the impact sites. We use a Markov chain Monte-Carlo algorithm in order to invert for lateral variations of crustal thickness on the Moon. The inversion uses travel times of seismic waves originating from multiple meteoroid impact locations. Previous seismic investigations constrained the crustal thickness solely for Apollo stations 12, 14 and 16, whereas our approach enables to estimate the crustal thickness at locations far from the Apollo network, and to build a first crustal thickness map based on seismic data. Here we compare our crustal thickness estimates based on seismic travel times to those based on inversions of the topography and gravity field. Both methods turn out to be coherent in the sense that highland sites possess a thicker crust than mare sites.

Keywords: lunar seismology; Apollo seismic data; crustal thickness; meteoroid impacts; gravity; topography

1. Introduction

The Moon is believed to have its origin in a giant impact event between the proto-Earth and an approximately Mars-sized body (e.g., [1–3]). The extreme amount of energy released during this catastrophic impact and the later reaccretion of debris in circum-terrestrial orbit was likely sufficient to melt a major portion of both bodies. Therefore, the Moon likely formed with a magma ocean whose depth could have ranged from ~250 km to the entire Moon [4,5]. One of the main outcomes of the Apollo sample analyses was to show that the lunar crust is anorthositic in composition, consistent with the differentiation of a magma ocean (e.g., [4,6]). While the resulting primary crust should be global in extent, its thickness was subsequently locally modified by major meteoroid impact events. As no Earth-like plate tectonic activity ever occurred after the formation of the lunar crust, these impacts are the main crustal reorganization process in the Moon's geologic evolution.

* Corresponding author. Present address: Etudes Spatiales et Planétologie, 4 avenue Neptune, 94100 Saint-Maur, France. Tel.: +33 1 45 11 42 57.
E-mail address: h.chenet@free.fr (H. Chenet).
[1] A portion of this work was accomplished while the author was at IPGP.
[2] Current address: Newton Press Inc., Nishi-Shinjuku 2-6-1, Shinjuku-ku, Tokyo, 163-0207, Japan.

0012-821X/$ - see front matter © 2006 Elsevier B.V. All rights reserved.
doi:10.1016/j.epsl.2005.12.017

Another significant modification of the lunar crust occurred with mare volcanism, which filled many of the near-side impact basins and the extensive region of Oceanus Procellarum. These flows are relatively thin and do not affect strongly the crustal thickness, having an average thickness of less than a kilometer exterior to basins, and possibly up to 6 km within the largest basins [7,8]. As elements such as aluminum, calcium, thorium and uranium were strongly partitioned into the crust during magma ocean crystallization, its mean thickness is a key parameter used to infer the global composition of the Moon (e.g., [9–13]).

To characterize the lunar crustal thickness, one typically makes use of the Apollo seismic data, or combined gravity and topography data. Previous investigations using seismic methods showed that the artificial impacts are the most convenient events to study the internal structure of the crust, as their source parameters are generally well known and because most of the corresponding seismic rays have their bottom point inside the crust. As a result of the sequential emplacement of the seismic stations, the number of data constraining the crustal structure beneath the Apollo sites decreases for Apollo 12, 14, 15 and 16. In addition, as a consequence of the relative proximity between the Apollo 12 and 14 stations (~180 km), these sites probably have a similar crustal structure. Based on these data, studies from the Apollo era proposed ~60 km crustal thickness estimates for the region of the Apollo 12 and 14 sites [14,15], which have since been used in almost all geophysical and geochemical models. However, this reference thickness was recently called into question by Khan et al. [16], Khan and Mosegaard [17] and Lognonné et al. [13], who proposed much thinner values of 45±5 km, 38±3 km and 30±2.5 km respectively, using different subsets of data (different events and arrival times were used in [13]) and different inversion techniques. Nevertheless, in these three 1-D models the artificial impacts near the Apollo 12 and 14 stations offer the tightest constraints on crustal structures and hence the above quoted values should be considered as being representative of this region only, and not of the bulk Moon. On the other hand, local investigations were performed at the Apollo 12 station with a receiver function method [13,18], and at the Apollo 16 station by analysis of multiple converted phases [19]. With the exception of the latter, none of these studies have addressed the issue of lateral crustal thickness variations.

In contrast to the previously mentioned seismic investigations, gravity and topography data obtained from the *Clementine* and *Lunar Prospector* missions allows one to address the question of lateral crustal thickness variations on a near-global scale (polar regions are not constrained). To construct such a crustal thickness map, the gravity signature due to the topography is subtracted from the observed field, yielding the Bouguer anomaly, and the remaining signal is then interpreted as relief along the crust–mantle interface, or lunar "Moho". However, such an inversion is non-unique in that one must assume values for the crustal and mantle density, as well as the crustal thickness at a single location. Typically, this anchoring point was taken to be ~60 km at the Apollo 12/14 site [20–22].

Lateral variations of topography and crustal thickness have not been simultaneously taken into account in previous seismological studies of the lunar interior. The only work which considered possible lateral heterogeneities was conducted by Khan and Mosegaard [17], where a time correction was considered at each station and impact site. Such corrections were introduced to

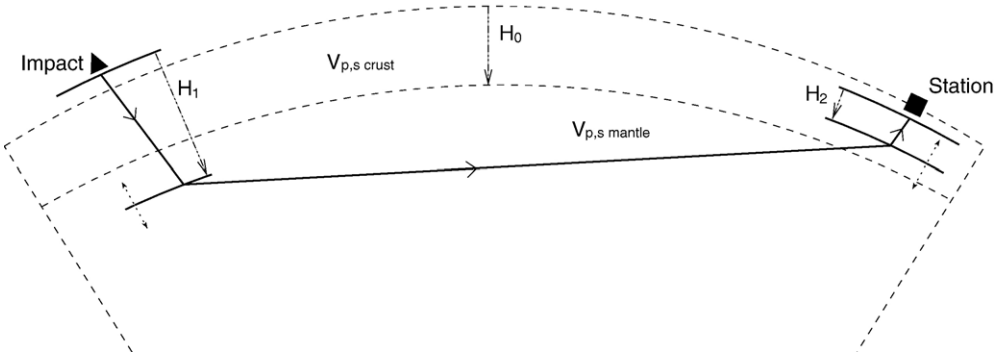

Fig. 1. Schematic seismic ray path from a meteoroid impact to an Apollo station in a model consisting of a single layer constant velocity crust. $V_{p,s}$ represents the constant P and S seismic velocities in the crust and mantle. The crust is sampled twice, once beneath the source and once beneath the receiver. H_0 is the reference crustal thickness. The depth of the crust–mantle interface is varied at the two sites to H_1 and H_2 in order to fit the observed arrival times. The topography of each site is explicitly considered in the calculations.

Table 1
Reference velocity model after Gagnepain-Beyneix et al. [28], with $V_p/V_s=1.75$

Depth	A		B		C	
	V_p	V_s	V_p	V_s	V_p	V_s
(km)	(km/s)		(km/s)		(km/s)	
0	4.6	2.63	1.0	0.57	1.0	0.57
1	4.6	2.63	1.0	0.57	1.0	0.57
1	4.6	2.63	5.22	2.98	4.15	2.37
10	4.6	2.63	5.22	2.98	4.15	2.37
10	4.6	2.63	5.22	2.98	5.04	2.88
17	4.6	2.63	5.22	2.98	5.04	2.88
17	4.6	2.63	5.22	2.98	6.00	3.43
24	4.6	2.63	5.22	2.98	6.00	3.43
24	4.6	2.63	5.22	2.98	6.85	3.92
30	4.6	2.63	5.22	2.98	6.85	3.92
30	7.57	4.33	7.57	4.33	7.57	4.33
500	7.57	4.33	7.57	4.33	7.57	4.33
500	8.26	4.65	8.26	4.65	8.26	4.65
1738	8.26	4.65	8.26	4.65	8.26	4.65

(A) Single layer crust; (B) single layer crust which considers a superficial low velocity layer; (C) crustal model consisting of 4 layers below the low velocity layer. Model B is used in the forward modeling.

compensate for the different elevations of the sites as well as possible lateral variations in thickness of the low velocity surficial layer.

In this paper, we propose to retrieve information about the thickness of the crust at different locations on the Moon by the use of the Apollo seismic data. To this end, we will make use of the artificial and natural meteoroid impacts. As these events occur at the surface, their seismic rays travel through the crust twice: once on the way down, and once on the way up (Fig. 1). The seismic signal generated by an impact thus contains information about the crustal structure beneath both the receiver and the impact site. The arrival time estimation for these events is not trivial because of the weak amplitude of the seismic wave arrivals, which is primarily a result of strong scattering processes in the upper crust [23,24]. Moreover, because seismic arrivals are not always discernible at all stations, the source location can not always be determined. As a consequence, only 19 of the 1743 events identified as meteoroid impacts in the Apollo data set [25] are usable in this study. Furthermore, we use here 7 of the 9 catalogued artificial impacts. Based on the limited number of suitable data, in the present study we choose to investigate only the lateral variations of crustal thickness, and not the velocity structure of the crust. The proposed strategy is thus to use a mean velocity model for the crust and mantle, and to model the arrival times by varying the thickness of the crust beneath the seismic stations and impact sites.

2. The data

The data employed here are the travel times of the impact events recorded during the Apollo Passive Seismic Experiment between 1969 and 1977 [25], as determined by Lognonné et al. [13]. The Apollo Seismic Network consists of four stations, one at each of the Apollo 12, 14, 15 and 16 sites. Detailed descriptions of the Apollo seismic data set and lunar seismology can be found in the extensive literature (e.g., [15,25–27] and references therein). Here we are interested in the impact data because their rays sample regions of the crust far from the Apollo sites, which is not the case of the deep moonquakes. Some shallow moonquakes may have occurred in the crust, but the depth uncertainty is too large to use these events in this study. The artificial events were generated by the impact of the Lunar Modules and the upper stage S-IVB of the Saturn V rockets with the lunar surface, and most of these correspond to relatively short epicentral distances ($<10°$ or $\sim$300 km). While the artificial impacts all occurred close to the Apollo stations, many of the meteoroid impacts occurred at larger epicentral distances from the Apollo network (see Fig. 6B).

Our study uses 7 artificial impacts, 19 meteoroid impacts, and 4 seismic stations. Dates, locations and arrival times for these impacts can be found in Tables 1 and 2 of Lognonné et al. [13]. The impact of the Apollo 16 S-IVB is not taken into account because its location was not accurately determined. For each ray path, the first P wave arrival is considered, as well as the S wave arrival when discernible. Because of the explosion-type source of the meteoroid impacts, the energy is released

Table 2
Parameters and crustal thickness results for the Apollo stations and the artificial impacts

Site	Lat (deg)	Lon (deg)	R_{topo} (km)	n_{data}	$\bar{H}_{crust}$ (km)	σ (km)
1 (A12)	−3.04	−23.42	1736.1	24	33.4	5.3
2 (A14)	−3.65	−17.48	1736.2	21	31.1	6.8
3 (A15)	26.08	3.66	1736.1	20	35.1	8.0
4 (A16)	−8.97	15.51	1737.6	19	38.0	6.8
5 (15 S-IVB)	−1.51	−11.81	1736.3	1	30.5	10.0
6 (17 S-IVB)	−4.21	−12.31	1736.2	3	39.9	5.6

primarily as compressional waves, i.e., P waves. Shear waves are weaker and thus fewer S wave arrivals are identified. In the best case scenario 208 arrival times would be available. However, our data set consists only of 102 readings, among which only one fifth are S wave arrivals. The reading errors attributed to the arrival time estimates are 1, 3 or 10 s [13] (cf. Fig. 3).

Of these 102 rays, those from impacts closest to the Apollo stations (<10°) do not sample the crust–mantle discontinuity because they are too shallow. 18 such arrival times of close impacts, concerning 11 sites, are thus excluded from our data set. As a consequence, the crustal thickness at five impact sites is not constrained at all by our data set and will not be investigated in the following. For one of the two artificial impacts remaining, only one useful arrival time exists, which makes the crustal thickness beneath these sites the least resolved of all in this study. This leaves us with a total of 25 sites and 84 useful arrival times at our disposal. The mean error of arrival time pickings for these is 4.6 s (cf. [13]). We label these sites as 1–4 for the Apollo stations, 5–6 for the artificial impacts and 7–25 for the natural impacts.

Here, we do not consider reflected or converted phases due to the crust–mantle or any other possible interfaces. This is in contrast to Toksöz et al. [14,15] whose main argument for a 60 km thick crust was in the interpretation of multiple P and S reflected waves. These identifications are controversial, as are the reflected phases identified in Goins et al. [19].

3. Monte-Carlo inversion

3.1. Forward modeling

Our goal is to define the best geometry of the lunar Moho relief explaining both the arrival time data of impact generated seismic waves and a mean velocity model of the crust and mantle. As previously mentioned, we use the same constant velocities for the crust and mantle at all the different impact sites and Apollo stations, and explore the effect of crustal thickness on the P and S wave arrival times. Of course, with such strong a priori information concerning the velocity structure, our results will therefore have to be considered in terms of crustal thickness variations relative to a mean thickness defined for a given velocity model. Another velocity model would lead to a different crustal thickness model.

In order to simplify the calculations of travel times, we define a single layer crustal model with a slowness equivalent to the slowness of the crustal model with a fixed V_p/V_s ratio proposed by Gagnepain-Beyneix et al. [28] (V_p=4.6 km/s and V_s=2.63 km/s) in an article following the paper by Lognonné et al. [13]. The mantle consists of two layers separated by a velocity discontinuity at 500 km depth. We fix the upper and lower mantle velocities to V_p=7.57 km/s, V_s=4.33 km/s, and V_p=8.26 km/s, V_s=4.65 km/s respectively (Table 1). These velocities correspond to an impedance ratio of V_p/V_s=1.75. Nevertheless, this ratio value for competent unfractured rocks might be inappropriate for the lunar crust, as the fractures caused by impact cratering are believed to increase the V_p/V_s ratio as deep as 30 km or more [13]. Therefore, we carried out inversions for different ratios in the crust, from V_p/V_s=1.75 to 2.0 (cf. Section 4). Moreover, other velocity models have been tested and will be discussed in the following section.

It is important to note here that we do not consider any lateral variations of seismic velocities in either the crust or mantle. While these might be present, the Apollo seismic database is too limited to place any meaningful limits on this parameter.

For the sites in our study, there is an almost 6 km range in surface elevations which corresponds to a maximum delay of ~1 and ~2 s for P and S wave travel times respectively. We therefore take the surface relief into account, using the absolute radii as measured by the LIDAR altimeter experiment onboard the Clementine spacecraft [29]. It is believed that the first few kilometers below the surface are composed of highly fractured materials that possess extremely slow seismic velocities [30]. Therefore, the mean crustal velocity is substantially diminished by the effect of these surficial layers, and this affects the geometry and travel times of non-vertical rays. In order to take this effect into account, we introduce a low velocity layer characterized by V_p=1.0 km/s. The V_s value depends on the V_p/V_s ratio chosen for the crust, and can possess values between 0.50 and 0.57 km/s. As no data exist that globally constrain the lateral variations of regolith thickness, we assume that the regolith layer (here "megaregolith") is uniform and parallel to the surface with a constant thickness of 1 km. Data obtained from the SELENE radar sounding experiment [31] may allow this effect to be taken into consideration in future models. Due to the large velocity gradient between the regolith layer and the basement, rays are almost vertical in this upper layer. We treat this effect by subtracting 1 km from all altitudes as well as 2 s from the P travel times. Depending on the V_p/V_s ratio, S travel times are reduced by 3.5 to 4 s. The P and S wave velocities of the remaining crust are then 5.22 km/s and $2.61 \le V_s \le 2.98$ km/s, respectively.

In contrast to this simple 1 layer crustal model, the seismic velocity is expected to increase with depth as a result of the closure of micro-fractures with increasing lithostatic pressure [14,32], possibly biassing the calculated raypaths. For rays with small epicentral distances, the assumption of a constant velocity crust could be grossly in error. Nevertheless, this error is likely to decrease with epicentral distance since the seismic rays will become increasingly more vertical within the crust. To quantify this effect, we computed the travel times in a single layer constant velocity crust and a more realistic crustal model possessing four layers (Table 1). We see in Fig. 2 that the travel time differences are small compared to the smallest arrival time error of 1 s for epicentral distances greater than 5°. Therefore, our single crust assumption will not affect significantly the computation of travel times for these epicentral distances. Moreover we simply ignore those impacts with epicentral distances smaller than 10°, because the seismic ray paths do not sample the crust–mantle discontinuity.

Given our assumption of constant velocity spherical shells, the raypaths are rectilinear. The travel times are analytically computed in each layer for a set of ray parameters and then summed. We use the relevant impact locations and origin times calculated from the velocity model of Lognonné et al. [13]. The typical error in the impact locations and time origins are approximately 3° and 3 s respectively (see Table 2 in [13]). We have performed an inversion with relocation, where the impact coordinates were explored together with crustal thickness, but this did not achieve a better fit to the data. Consequently final inversions described in next section do not relocate the events.

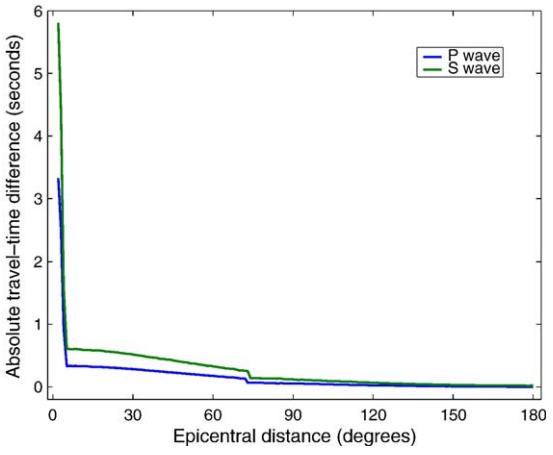

Fig. 2. Difference in travel times between a single layer crust and a crustal model with 4 homogeneous layers possessing a realistic positive velocity gradient with depth. Time differences between these two models are plotted as a function of epicentral distance, for both P (blue) and S (green) waves. The discontinuity at 75° is related to a sharp change in velocity at 500 km depth in the mantle. For epicentral distances above 5°, the time differences are smaller than the smallest arrival time uncertainty of 1 s.

3.2. Inverse problem

Our parameterization consists of a set of 25 sites, each defined by a different surface elevation and a variable depth of the crust–mantle boundary. Our inversion for the crustal thickness at each site H^i_{crust}, is based on a Markov chain Monte-Carlo algorithm (MCMC), similar to the one used by Khan and Mosegaard [17] in their 1D inversion of the lunar velocity structure (see also Tarantola and Valette [33] and Mosegaard and Tarantola [34]). In essence, the method extensively explores the model space accordingly to the posterior probability distribution, via a random walk. Further details can be found in Appendix A.

Let $\boldsymbol{m}_{\mathrm{cur}}$ be the current set of 25 crustal thicknesses H^i_{crust} at the start of the random walk, and let $\boldsymbol{m}_{\mathrm{pert}}$ be the model vector after a perturbation of one of its components. The selection of the site to be perturbed is random, as well as the perturbation of the depth of the crust–mantle interface. The upper limit of the Moho is constrained to be less than the surface elevation, i.e., $H^i_{\mathrm{crust}} \geq 0$. Discrepant crustal thicknesses of neighboring sites are further penalized through a correlation function that is controlled by a correlation length of 5°, and a mean crustal thickness of 40 ± 15 km. The effect of the mean crustal thickness penalization is to weaken the probability of models where all the stations are on a thick crust and impacts sites on a thin crust or vice versa. By exploring various values of correlation length and mean crustal thickness, and by running an inversion that did not employ the correlation in the misfit function, we have found that this a priori information precludes the sampling of unrealistic models and reduces the uncertainty for crustal thickness estimates (as measured by the marginal posterior probability distributions) by ~ 3 km.

Each iteration consists of a perturbation of one H^i_{crust}, followed by the computation of the travel times $\boldsymbol{d}_{\mathrm{calc}}$ corresponding to the set of model parameters $\boldsymbol{m}_{\mathrm{pert}}$. The likelihood function is then calculated, which is a measure of the misfit between $\boldsymbol{d}_{\mathrm{calc}}$ and observed data, $\boldsymbol{d}_{\mathrm{obs}}$. Then the perturbation is accepted with a prescribed probability that depends on the improvement this model brings to the data fit (cf. Appendix A).

4. Results

In order to test the sensitivity of our modeling procedure to crustal thickness variations, we first invert synthetic crustal thickness data for the 25 sites (2 artificial impacts + 19 meteoroid impacts + 4 Apollo stations). The four Apollo stations are much better sampled than the impact sites (21 times more on average), and each impact does not possess the same number of arrival time readings (between 1 and 6). Moreover, as the reading uncertainties can be high, the model resolution is expected to be highly variable among the sites. Many synthetic inversions were performed in order to calibrate the random walk parameters correctly. We show here the results of a particular test where synthetic data were perturbed from the original data using the measured observational errors of observed arrival times.

Results are expressed as crustal thickness marginal posterior probability distributions, and represented with a color-scale in Fig. 3. The marginal probability of a particular event $m_j = H^j_{\text{crust}}$ is the probability that m_j occurs regardless of all possible values of other parameters $\boldsymbol{m}' = H^{i\neq j}_{\text{crust}}$, i.e.

$$\mathcal{P}(m_j) = \int_0^\infty \Phi(m_j, \boldsymbol{m}')\mathrm{d}\boldsymbol{m}' \quad (1)$$

($\Phi(\boldsymbol{m})$ is explained in Appendix A).

Fig. 3 shows the uncertainties of the arrival time readings for all impact sites and stations, demonstrating how both the number of readings and their associated uncertainties affect the posterior probability distributions. As expected, this test shows that the sites constrained by fewer arrival time readings and/or large reading errors generally possess the largest posterior errors (see Fig. 3). This is especially the case of impacts 11, 12, 16, 18, 21, 25, which show relatively uniform probability distributions. While the inversion results for sites 18 and 25 are not concordant with the input values, synthetic tests show that the agreement is improved for these two sites by using smaller perturbations.

We now discuss the results of our inversion of real data, having used the velocity model "B" described in

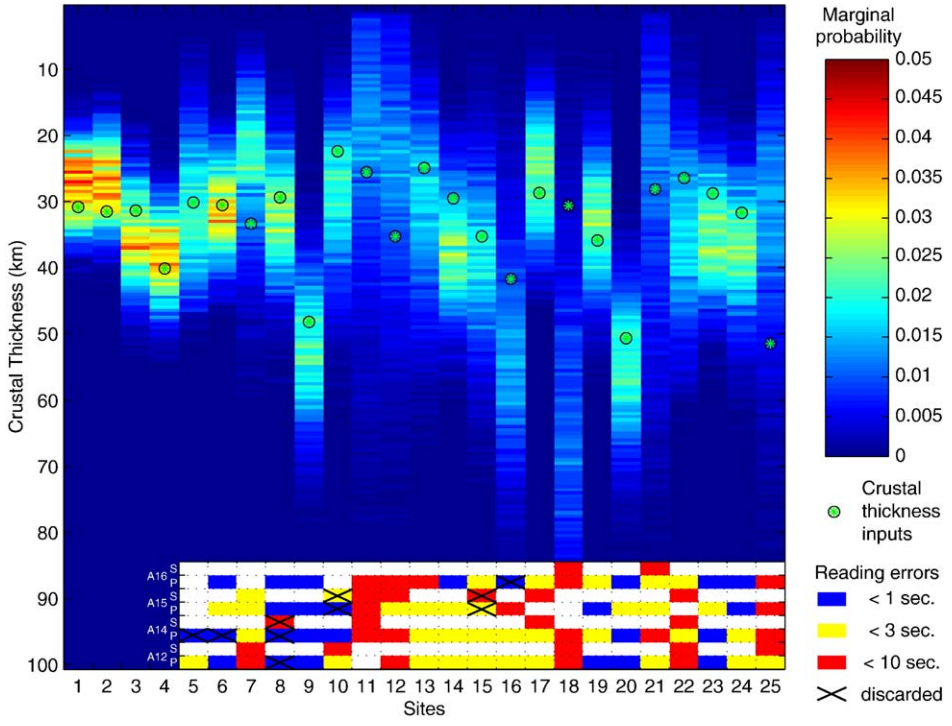

Fig. 3. Effect of the number and quality of data on the robustness of the inversion. Background figure: marginal posterior probability distributions of crustal thicknesses for a synthetic test where "observed" arrival times were perturbed according to the actual arrival times reading errors. Sites 1 to 4 represent the Apollo stations 12, 14, 15 and 16, whereas sites 5–25 are for the 21 impact sites. Green stars circled in black represent the crustal thickness inputs at each site. Foreground: table displaying the observed arrival time uncertainties, for each impact relative to stations and type of seismic wave (P or S). Arrival times corresponding to epicentral distances shorter than 10° were discarded.

Table 1 (V_p/V_s=1.75). Fig. 4 shows the obtained marginal posterior probability distribution for each site, whose details are reported in Tables 2 and 3.

For each location, the mean and standard deviation of the crustal thickness is determined from the posterior probability distribution. $\bar{H}_{crust}$ varies between ~23 km and ~66 km, and the average crustal thickness seen by the 25 sites is 38.3±12.6 km. As explained earlier, the Apollo sites are the best constrained among the sites in this study as a result of being sampled by a larger number of seismic rays. From our exploration, we can propose crustal thicknesses of 33±5 km, 31±7 km, 35±8 km, and 38±7 km respectively for Apollo stations 12, 14, 15 and 16 (sites numbered 1, 2, 3 and 4). Crustal thickness variations are indeed present within the region of the crust spanned by the four Apollo stations. As suspected because of their proximity (~180 km), the Apollo 12 and 14 station sites do not differ appreciably in terms of their crustal thickness. The Apollo 15 site has a slightly larger value than the 12 and 14 sites. The Apollo 16 site possesses the thickest crust (38±7 km) among the four stations, which is consistent with its higher elevation and the hypothesis of Airy compensation. A similar relative pattern was proposed by Goins et al. [19] with a crustal thickness of ~75 km at this site as opposed to ~60 km for Apollo 12 and 14, based on the putative identification of converted phases. Considering the modest crustal thickness variations that we find for the Apollo 12, 14 and 15 sites, and the fact that the Apollo 16 site possesses the shortest span of data due to its time of emplacement, we finally note that the hypothesis of a constant crustal thickness beneath the Apollo zone, as was used in previous seismic studies, is likely to be a decent approximation.

Among the 21 impact sites, we can distinguish some particular sites (such as 7, 11, 12, 13, 15, 16, 18, 21, 25) which show relatively uniform probability distributions (cold blue colors). This was expected based on our synthetic tests (Fig. 3), and is a result of both the limited number of data and the large uncertainties in the arrival time readings. Site 6 is seen to have the most peaked distribution among the impacts, and is characterized by a 40±6 km crustal thickness. This is considerably thicker than the Apollo 14 site (31±7 km), which is only 155 km away.

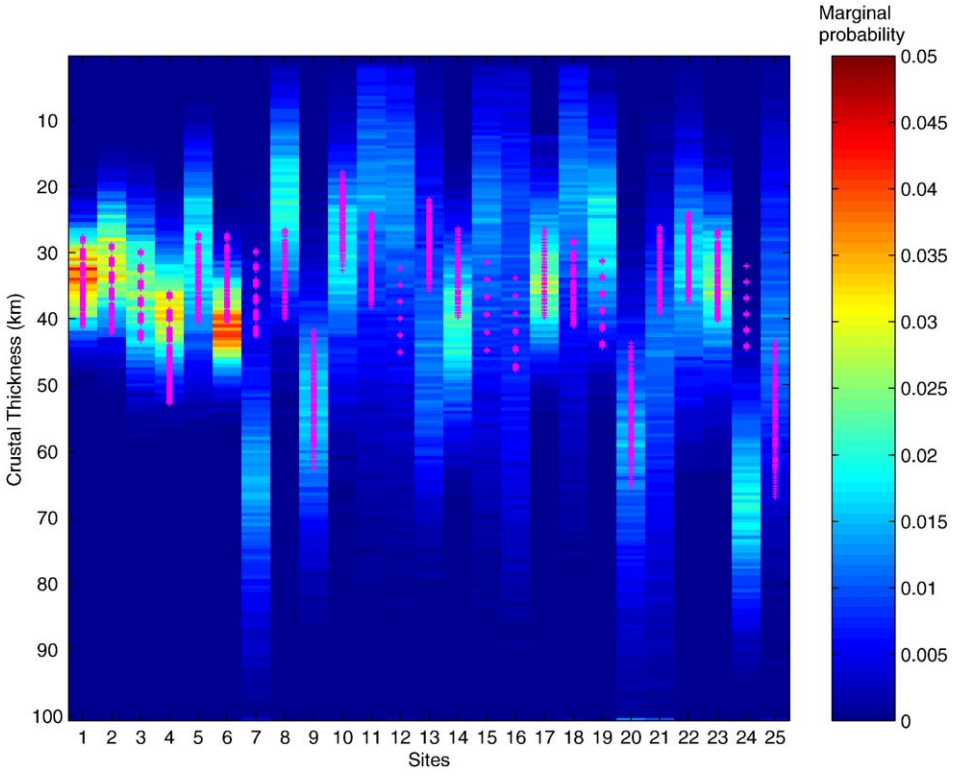

Fig. 4. Results of the inversion of 84 real data for the 25 sites, expressed as crustal thickness marginal probability distributions. Superposed to these distributions, the magenta crosses depict all the gravity models coherent with the seismic data within two standard deviation as determined by a chi-squared analysis (see Section 5 and Fig. 5).

Table 3
Results for the meteoroid impacts (sites 7–25)

Site	Year/month/day	Lat (deg)	Lon (deg)	R_{topo} (km)	n_{data}	$\bar{H}_{crust}$ (km)	σ (km)
7	1972/01/04	74.10	2.60	1736.7	5	60.8	16.8
8	1972/05/13	1.50	−17.10	1736.4	2	23.0	10.0
9	1972/07/17	32.80	137.60	1740.7	4	53.2	12.9
10	1972/07/31	24.00	10.10	1734.8	3	31.3	12.1
11	1972/08/29	15.80	22.90	1736.3	5	27.9	17.1
12	1973/09/26	28.70	41.10	1738.0	5	29.5	17.7
13	1973/12/24	−24.80	−25.10	1735.4	4	40.8	16.5
14	1974/04/19	7.40	−33.60	1736.3	4	40.3	9.7
15	1974/07/17	20.30	6.50	1736.5	3	32.4	17.1
16	1974/11/21	−7.30	19.90	1738.1	3	37.9	19.9
17	1974/12/15	1.60	−8.20	1736.5	5	32.8	8.4
18	1975/03/05	−52.40	4.20	1736.5	5	28.5	17.5
19	1975/04/12	2.00	43.20	1737.7	4	26.7	10.3
20	1975/05/04	−36.40	−121.30	1739.3	4	59.8	15.9
21	1976/01/13	−39.40	62.80	1736.3	5	50.0	19.3
22	1976/05/28	−16.80	−10.00	1735.4	6	32.5	12.1
23	1976/11/14	23.80	−73.90	1736.0	4	34.8	9.4
24	1977/04/17	−20.50	−63.80	1737.1	4	66.3	11.4
25	1977/06/28	−13.50	−75.0	1740.8	5	41.1	17.5

Finally, we show our results on a lunar map, in Fig. 6A. Here, the color represents the crustal thickness, and the size of each point is inversely proportional to its uncertainty. We remark that those sites which are located in the highlands possess the largest crustal thicknesses, and that the thinnest values are found in the lunar maria.

As explained previously, the inversion that we just described considers a V_p/V_s ratio of 1.75. However, this ratio could possibly have a higher value in the crust [13]. Therefore we carried out two other inversions using the same V_p model, but with V_p/V_s ratios of 1.875 and 2.0. In both cases, the results are not substantially different, essentially because our data set mainly consists of P wave arrivals. The estimates of crustal thickness do not deviate much from the $V_p/V_s=1.75$ run, and stay largely within the error bars of the previous inversion. The mean difference of crustal thickness between the $V_p/V_s=1.75$ run and the $V_p/V_s=1.875$ run is 1.1 km, while it reaches 2.3 km for $V_p/V_s=2.0$. The only significant difference is for site 7, where the crust is seen to be 40 ± 20 km for $V_p/V_s=2.0$ compared to 61 ± 17 km thick for $V_p/V_s=1.75$. The great similarity between these tests shows that our results are not significantly affected by this assumed impedance ratio.

On the other hand, to take into account the uncertainties of the different models proposed by Gagnepain-Beyneix et al. [28], we also carried out inversions with higher velocities in the upper mantle and lower velocities in the crust. We used a model with $V_p=4.65$ km/s and $V_s=2.66$ km/s in the crust, and $V_p=7.7$ km/s and $V_s=4.4$ km/s in the upper mantle (to be compared with $V_p=5.22$ km/s and $V_s=2.98$ km/s in the crust, and $V_p=7.57$ km/s and $V_s=4.33$ km/s in the mantle for the model described in the previous section). Using this model produces similar distributions than the first model we used. Differences in posterior probability distributions of crustal thickness are minor in comparison with the standard deviations. However, lower mantle velocities appear to control the determination of crustal thickness at distant sites. We tested several velocities and it is clear that the crustal thickness of far side highland sites is significantly larger than for the mare sites only if the lower mantle P velocities are larger than $V_p\sim8.15$ km/s.

5. Comparison between seismic and gravity based crustal thicknesses

As mentioned in the Introduction, an alternative method of estimating the thickness of the lunar crust is based upon the analysis of gravity and topography data. While methods do exist for estimating the average crustal thickness using these data sets (e.g., [35]), most investigations simply fix the average thickness such that the seismically measured value at the Apollo 12/14 site is satisfied. The purpose of this section is to determine which sets of parameters employed by the gravity-based models most accurately fit the seismic constraints calculated in the previous section.

Similar to our seismic models, the gravity models consist of a single layer crust overlying a mantle, each of which possesses a constant density. While more complicated crustal models could be envisioned, Wieczorek and Phillips [22] have found that the total crustal thickness of a dual layered-crust does not differ significantly from a single layered model. The crust and mantle densities, as well as the assumed average crustal thickness, uniquely determine the Moho relief in the models. As one uses thinner average crustal thicknesses, the density contrast between the crust and mantle generally needs to be larger in order to obtain physically reasonable solutions (i.e., the crustal thickness can not be negative). While the crustal and mantle densities of the Moon are not perfectly known, a variety of sources of information can be used to place reasonable limits on these parameters.

For a set of parameters ρ_C (crustal density), ρ_M (mantle density) and H^0_{crust} (mean crustal thickness), we construct a crustal thickness map following the methodology of Wieczorek and Phillips [22]. The mare basalts within the large basins are taken into account, being based upon the model of Solomon and Head [36] and modified by the maximum basalt thicknesses of Williams and Zuber [8]. Contrary to previous studies, the Bouguer correction is not filtered, as the power spectrum of the LP150Q [37] gravity model is realistic up to degree 65. The gravity and topography fields are only used up to degree 65, and in inverting for crustal thickness, the downward continuation filter of Wieczorek and Phillips [22] is used such that this filter has a value of 0.5 at degree 30. The relief of the crust–mantle interface is calculated in an iterative manner until the maximum difference between iterations is less than 75 m (see [22] and [38] for more details).

We construct a large set of gravity based crustal thickness maps that evenly sample the ρ_C, ρ_M and H^0_{crust} parameter space. In particular, crustal density is varied from 2600 to 3200 kg/m 3 in steps of 50 kg/m 3, mantle density from 3250 to 3450 kg/m 3 in steps of 50 kg/m^3, and H^0_{crust} from 25 km to 70 km in steps of 2.5 km. We then compare the 25 crustal thicknesses found in our previous seismic inversion with the values predicted from each gravity inversion. Those models that yield unphysical solutions, such as negative crustal thicknesses, were ignored. In all, this leads to the consideration of a total of 545 individual gravity-based models.

We quantify the misfit between the *gravity* and *seismic* models by use of a chi-squared function. For each set of parameters used in constructing a gravity-based crustal thickness map (here indexed by $j=1$ to 545), the chi-squared misfit is calculated according to

$$\chi^2_j = \sum_{i=1}^{n=25} \frac{[H_s(i) - H^j_g(i)]^2}{\sigma^2_s(i)} \quad (2)$$

where $\boldsymbol{H}_s$ and $\boldsymbol{\sigma}_s$ are the average crustal thickness and standard deviation at the 25 impact sites based on our seismic inversion (Tables 2 and 3), and $\boldsymbol{H}^j_g$ are the corresponding values from the gravity inversions. The number of degrees of freedom is given by $\nu=n-M$, where n is the number of sites ($n=25$) and M is the number of free parameters ($M=3$). If the uncertainties for the seismic-based average crustal thicknesses, $\boldsymbol{H}_s$, are Gaussian distributed, then the expectation of χ^2 is ν, with a standard deviation of $\sigma_{\chi^2} = \sqrt{2\nu}$ (e.g., [39], p. 654). Equivalently, the expectation of the reduced chi-squared, $\chi^2_\nu = \chi^2/\nu$, is 1 with a standard deviation of $\sigma_{\chi^2/\nu} = \sqrt{2/\nu}$. For our case with $n=25$ and $M=3$, $\sigma^2_{\chi/\nu}=0.3$.

Fig. 5 shows the reduced chi-squared as a function of ρ_C and H_0, plotted separately for the different values of ρ_M. The minimum χ^2/ν is 0.7. As an estimate of the uncertainty on the parameters ρ_C, ρ_M and H_0, we take those models with $\chi^2/\nu \le \chi^2_{min}/\nu + 2\sigma^2_{\chi/\nu} = 1.3$ as being acceptable. This corresponds to H_0 spanning from 32.5 to 45 km, with a best fit of $H_0=40$ km. ρ_C is constrained to be less than 2900 kg/m^3, with the lower values being preferred. This is consistent with the composition of central peaks which sample materials up to 30 km below the surface [10]. In particular, Wieczorek and Zuber [10] estimated the pore-fee density of the upper and most mafic portions of the lower crust to be about 2855 and 3038 kg/m^3, respectively. Reducing these by 5% to take into account porosity gives 2710 and 2885. All values of ρ_M give acceptable solutions. All of the acceptable models are plotted for our 25 sites in Fig. 4, over the results obtained from the seismic analysis.

Fig. 6B displays a typical well-fitting gravity-based crustal thickness map for the parameters $\rho_C=2800$ kg/m^3, $\rho_M=3350$ kg/m^3 and $H_0=40$ km. We note that this model possesses minimum and maximum crustal thicknesses of ~2 km beneath the Crisium Basin, and ~100 km in the far-side highlands. For comparison, the impact sites used in the seismic investigation are shown, and the seismic map in Fig. 6A uses the same color scale as the gravity-based map. A visual comparison between Fig. 6A and B shows a fairly good consistency for most sites when the uncertainty in the seismic value is taken into consideration.

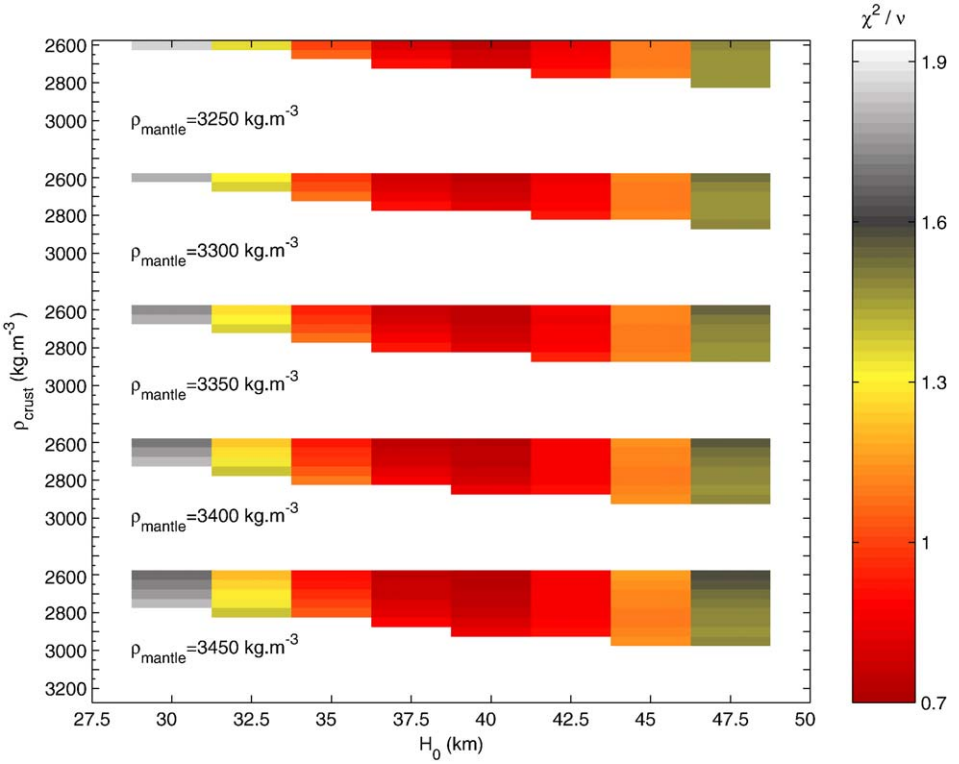

Fig. 5. Reduced chi-squared misfit between the seismic crustal thickness estimates and a suite of gravity models that depend upon ρ_C, ρ_M and H_0. χ^2_{min}/ν and $\sigma^2_{\chi/nu}$ are respectively equal to 0.7 and 0.3. Only models with a fit better than four standard deviations are displayed. We consider those models that lie within two standard deviations (red to yellow colors) of χ^2_{min}/ν to be acceptable solutions.

Regarding the Apollo stations (sites 1–4), which are the best constrained sites from the seismic analysis, a good agreement is seen between the two methods (see Figs. 4 and 6). Our seismic inversion gives 33±5 km, 31±7 km, 35±8 km, and 38±7 km for the Apollo stations 12, 14, 15 and 16, respectively, while the gravity-based models respectively range from 28 to 41 km, 29 to 42 km, 30 to 43 km, 36 to 53 km, showing that the two methods are consistent within uncertainties.

Sites 9 and 20 are the farthest points from the Apollo network, located on the far side respectively at (32.8N, 137.6E) and (36.4S, 121.3W). Together with site 25, which lies on the western limb, these highland sites are predicted to lie on a "thick" crust by all the accepted gravity maps. In particular for sites 9, 20 and 25, we obtain values of 42–63 km, 44–65 km, and 43–67 km respectively (see Fig. 4). Accordingly, seismic estimates for sites 9 and 20 are 53±13 km and 60±16 km respectively, but site 25, which is resolved by unclear seismic arrival times (Fig. 3), does not show such a good agreement (H_s=41±18 km). As a possible explanation for this discrepancy, we note that site 25 has the largest location uncertainty among the impacts (7°) as a consequence of the considerable arrival time errors for this site (Fig. 3). Thus, it is possible that site 25 in fact lies outside of the rather isolated thick crustal region as predicted by gravity-based model, which would solve the discrepancy (Fig. 6).

Because the seismic rays sample deeper with increasing epicentral distances, the crustal thickening away from the Apollo network and the velocity increase in the deep mantle are closely related. Tests showed that the far side crustal thicknesses are controlled by the lower mantle velocity: a rather large velocity (V_p>8.15 km/s) gives rise to crustal thicknesses larger than for the near side maria. If the only mantle discontinuity is at 500 km depth, then this only affects sites with epicentral distances greater than 100° away from the Apollo stations. If the thickening of the crust away from the network is real, as the gravity/topography data suggest on the far side, then it also indicates that the velocity in the deep mantle should be significantly larger than in the upper mantle, as explained earlier.

The strongest dissimilarities between both maps are for sites 7 and 24: the seismic values seem relatively thick, 61±17 km and 66±11 km respectively, compared to the thinner values of 30–43 km and 32–44 km as estimated from the gravity-based map. These predictions

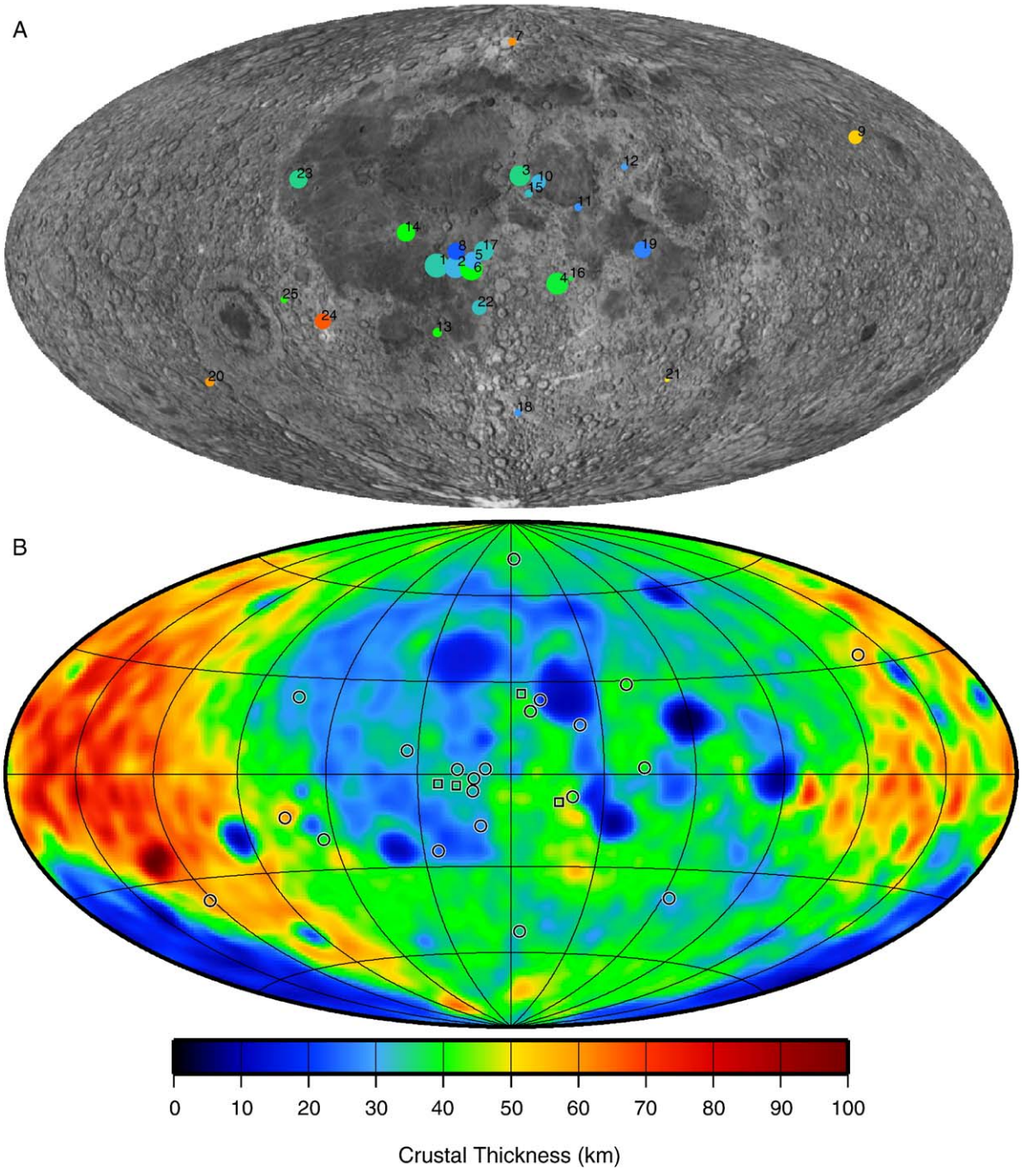

Fig. 6. Crustal thickness maps based on A) seismic and B) gravity data. In A) the symbol size is inversely proportional to their uncertainty. Crustal thickness map in B) corresponds to parameters $\rho_C = 2800$ kg/m^3, $\rho_M = 3350$ kg/m^3 and $H_0 = 40$ km. Squares are for the four Apollo stations (sites 1, 2, 3 and 4).

are incompatible given the uncertainties of our estimates. Nevertheless, tests show that a higher crustal impedance ratio ($V_p/V_s = 2.0$) would lead to a much thinner estimate for site 7 (40 ± 20 km), while only having a minor affect on the other seismic-based crustal thickness estimates.

6. Conclusion

In order to address lateral variations of crustal thickness, we used the seismic wave arrivals of the meteoroid impacts, which carry a unique signature of

the crust at sites far from the Apollo stations. The major limitation of such a study comes from the problematic detection of these meteoroid impacts, whose seismic arrivals are often highly uncertain. The utilization of other kinds of events such as the shallow and deep moonquakes, as was done by Toksöz et al. [15], Goins et al. [40], Nakamura [41], Khan and Mosegaard [17] and Lognonné et al. [13] to build up mean velocity models, is complementary to our approach, and in some sense necessary as our assumed constant seismic velocity layers for the crust and mantle are based upon these previous studies. This analysis yielded 25 crustal thickness estimates, some of them located more than 3000 km from the Apollo stations.

In contrast to the seismic method, lateral variations in crustal thickness can be estimated from the inversion of gravity and topography fields. This approach has the main advantage of being able to estimate crustal thickness everywhere, but suffers from both the non-unicity of the interpretation of potential fields and to a lesser extent the reliability of the lunar gravity and topography fields. In particular, it is necessary to assume constant densities for the crust and mantle, as well as an average crustal thickness. For this purpose, a comparison between the gravity based method and seismic data was used to constrain these three parameters. A good first order agreement was found between the two methods, with coherent relative thicknesses for the Apollo 12, 14, 15 and 16 sites: 33±5 km, 31±7 km, 35±8 km, and 38±7 km respectively, according to the seismic analysis. The crust beneath the Apollo 12, 14, and 15 sites appears to have similar thickness, whereas station 16 exhibits a thicker crust, as might be expected given its higher elevation. Nevertheless, the relative thickness differences among the Apollo sites are rather modest when compared to the totality of our results.

The majority of available data comes from impacts on the Oceanus Procellarum region, mostly on mare units;[3] we find that the crustal thickness there is relatively thin, with values between ~25 and ~40 km. On the other hand, two impacts clearly identified as far side highland sites[4] possess a considerably thicker crust of ~55–60 km. This thickening of the crust away from the Apollo network is consistent with the velocity increase in the deep mantle.

In conclusion, we considered both the locations of surface sources and receivers as relevant sites to investigate the local crustal thickness. In this way, we could address for the first time lateral variations of lunar crustal thickness with seismic data. The picture of the crust that we draw makes possible the first comparison of the combined gravity/topography analysis with the study of seismic data, and indeed we have shown that they are generally consistent. If we consider an upper mantle velocity of V_p=7.57 km/s, the most probable estimate for a mean lunar crustal thickness is 40±5 km, with crustal densities less than 2900 kg/m^3. Finally, it is important to note that the major hindrance of our seismic approach on the crustal thickness issue, like all previous studies, is the difficulty to determine precise seismic arrival times for a majority of seismic events. As a consequence of this, only 19 natural impact data were used in this study, whereas 1743 meteoroid impacts have been identified in the Apollo data set [25]. A new extensive network on both lunar sides would unquestionably solve the problem of identifying the numerous seismic sources available on the Moon, those being a key to understanding the lunar interior.

[3] Sites 1, 2, 3, 5, 6, 8, 10, 11, 12, 13, 14, 15, 17, 19, 22 and 23.
[4] Sites 9 and 20.

Acknowledgments

The authors would like to thank Pr. Yosio Nakamura for his perspicacious and helpful review. We appreciated the fruitful discussions with Amir Khan about the MCMC algorithm and Jeannine Gagnepain-Beyneix concerning the Apollo seismic data set. H. Chenet is supported by the Japan Society for Promotion of Science. This work was funded by CNES and by PNP. Additional support has been provided by the European Commission's Improving Human Potential Program under contract RIN2-2001-00414, MAGE. This is IPGP contribution 2110.

Appendix A. Initialization of the random walk

A starting model m is introduced, defined by

$$\boldsymbol{m} = (H^1_{\text{crust}}, \ldots, H^i_{\text{crust}}, \ldots, H^n_{\text{crust}}) \quad (3)$$

where the H^i_{crust} correspond to the depth of the lunar Moho at the n=25 impact sites.

Appendix B. Random walk

B.1. Start of the random walk

The calculated data $\boldsymbol{d}_{\text{calc}}=g(\boldsymbol{m}_{\text{cur}})$, consisting of N travel times, are computed by a forward algorithm for the model $\boldsymbol{m}_{\text{cur}}$, and then compared to observations

$\boldsymbol{d}_{\text{obs}}$ through the use of the likelihood function defined as

$$L(\boldsymbol{m}) = k \cdot \exp(-S(\boldsymbol{m})) \tag{4}$$

where k is constant and the misfit between the model and observation is estimated by

$$S(\boldsymbol{m}) = \sum_{i=1}^{N} |g^i(\boldsymbol{m}) - d^i_{\text{obs}}|/\sigma_i \tag{5}$$

where σ_i is the uncertainty on the ith arrival time. The misfit function is here computed via an l_1 norm, which is more reliable than an l_2 norm when outliers are present in the data set [42].

B.2. Perturbation

One site is randomly chosen within the $n=25$ sites, and the corresponding crust–mantle boundary is randomly perturbed, giving rise to a new model $\boldsymbol{m}_{\text{pert}}$, for which new travel times $\boldsymbol{d}_{\text{calc}}=g(\boldsymbol{m}_{\text{pert}})$ are computed.

B.3. Correlation

We introduce a priori information through

$$\rho(\boldsymbol{m}) = \zeta \cdot \exp(-S_{\text{prior}}(\boldsymbol{m})) \tag{6}$$

where ζ is a constant, in order to favor a relative continuity of the Moho shape at short wavelengths. This is operated via a correlation function characterized by a crustal thickness standard deviation a and a correlation length L_{corr}

$$C_L(i,j) = \alpha^2 \exp\left[-\frac{\delta(i,j)^2}{2L^2_{\text{corr}}}\right] \tag{7}$$

where δ is the distance between two different sites i and j.

The misfit between the model and the prior information is then given by

$$S_{\text{prior}}(\boldsymbol{m}) = [(H^i_{\text{crust}} - H^0_{\text{crust}})^T \cdot C_L^{-1}(i,j) \cdot (H^j_{\text{crust}} - H^0_{\text{crust}})] \tag{8}$$

where H^0_{crust} is the mean Moho radius, and H^i_{crust} and H^j_{crust} the Moho radii for the two sites indexed by i and j. Sites that are close to each other and that have different crustal thicknesses will therefore be penalized. The posterior probability density $\Phi(\mathbf{m})$ is thus sampled (η being a constant):

$$\Phi(\boldsymbol{m}_{\text{pert}}) = \eta\rho(\boldsymbol{m}_{\text{pert}})L(\boldsymbol{m}_{\text{pert}}) \tag{9}$$

B.4. Acceptance/rejection

The next step is to decide whether the perturbation should be accepted or not, and with what probability. The comparison between $\boldsymbol{m}_{\text{pert}}$ and $\boldsymbol{m}_{\text{cur}}$ is performed using the Metropolis criterion [43], which assesses a probability of acceptance P_{accept} following

$$P_{\text{accept}} = \min\left(1, \frac{L(\boldsymbol{m}_{\text{pert}})}{L(\boldsymbol{m}_{\text{cur}})}\right) \tag{10}$$

Simply, a "good" perturbation is automatically accepted ($P_{\text{accept}}=1$), whereas a "bad" perturbation [$L(\boldsymbol{m}_{\text{pert}})<L(\boldsymbol{m}_{\text{cur}})$] can also be accepted, but with a lower probability equal to $L(\boldsymbol{m}_{\text{pert}})/L(\boldsymbol{m}_{\text{cur}})$. If $\boldsymbol{m}_{\text{pert}}$ is finally accepted, the perturbed model becomes the current model $\boldsymbol{m}_{\text{cur}}$ to be perturbed again in step (B.2) for a next iteration. If $\boldsymbol{m}_{\text{pert}}$ is rejected, $\boldsymbol{m}_{\text{cur}}$ from current iteration is conserved for another (B.2) perturbation step.

Appendix C. Convergence

The above iterative process converges towards models which are globally more and more coherent with the observed data. The rate at which convergence occurs depends on the characteristic length of perturbation in the random walk steps, and optimal values were obtained through a series of tests on synthetic and real data (see Fig. 3 for results of a synthetic test). This process B.2→B.4 is repeated until the model space is sufficiently sampled; we stop the exploration after 500,000 iterations.

References

[1] A.G.W. Cameron, Higher-resolution simulations of the Giant Impact, in: R.M. Canup, K. Righter (Eds.), Origin of the Earth and Moon, Univ. of Arizona Press, Tucson, Arizona, 2000, pp. 133–144.
[2] R.M. Canup, E. Asphaug, Origin of the Moon in a giant impact near the end of the Earth's formation, Nature 412 (2001) 708–712.
[3] R.M. Canup, Simulations of a late lunar-forming impact, Icarus 168 (2004) 433–456.
[4] P.H. Warren, The magma ocean concept and lunar evolution, Annu. Rev. Earth Planet. Sci. 13 (1985) 201–240.
[5] M.E. Pritchard, D.J. Stevenson, Thermal aspects of a lunar origin by giant impact, in: R.M. Canup, K. Righter (Eds.), Origin of the Earth and Moon, Univ. of Arizona Press, Tucson, AZ, 2000, pp. 179–196.
[6] S.R. Taylor, Planetary Science: A Lunar Perspective, Lunar and Planetary Institute, Houston, 1982, 481 pp.
[7] R.A. De Hon, Thickness of the western mare basalts, Proc. Lunar Planet. Sci. Conf. 10th, 1979, pp. 2935–2955.
[8] K.K. Williams, M.T. Zuber, Measurements and analysis of lunar basin deposits from Clementine altimetry, Icarus 131 (1998) 107–122.

[9] B.L. Jolliff, J.J. Gillis, L.A. Haskin, R.L. Korotev, M.A. Wieczorek, Major lunar crustal terranes: surface expressions and crust–mantle origins, J. Geophys. Res. 105 (2000) 4197–4216.
[10] M.A. Wieczorek, M.T. Zuber, The composition and origin of the lunar crust: constraints from central peaks and crustal thickness modeling, Geophys. Res. Lett. 28 (21) (2001) 4023–4026.
[11] P.H. Warren, Compositional structure within the lunar crust as constrained by lunar prospector Thorium data, Geophys. Res. Lett. 28 (13) (2001) 2565–2568.
[12] S.R. Taylor, The moon, in: S.R. Taylor (Ed.), Solar System Evolution, a New Perspective, Cambridge University Press, Cambridge, UK, 2001, pp. 369–399.
[13] P. Lognonné, J. Gagnepain-Beyneix, H. Chenet, A new seismic model of the Moon: implications for structure, thermal evolution and formation of the Moon, Earth Planet. Sci. Lett. 211 (2003) 27–44.
[14] N.M. Toksöz, F. Press, A. Dainty, K. Anderson, G. Latham, M. Ewing, J. Dorman, D. Lammlein, G. Sutton, F. Duennebier, Structure, composition and properties of the lunar crust, Proc. Third Lunar Sci. Conf., Geochim. Cosmochim. Acta, Suppl., vol. 3, 1972, pp. 2527–2544.
[15] N. Toksöz, A. Dainty, S. Solomon, K. Anderson, Structure of the Moon, Rev. Geophys. Space Phys. 12 (1974) 539–567.
[16] A. Khan, K. Mosegaard, K.L. Rasmussen, A new seismic velocity model for the Moon from a Monte Carlo inversion of the Apollo lunar seismic data, Geophys. Res. Lett. 27 (2000) 1591–1594.
[17] A. Khan, K. Mosegaard, An inquiry into the lunar interior: a nonlinear inversion of the Apollo lunar seismic data, J. Geophys. Res. 107 (2002), doi:10.1029/2001JE001658.
[18] L.P. Vinnik, H. Chenet, J. Gagnepain-Beyneix, P. Lognonné, First seismic receiver functions on the Moon, Geophys. Res. Lett. 28 (15) (2001) 3031–3034.
[19] N. Goins, A. Dainty, N. Toksöz, Structure of the lunar crust at highland site Apollo station 16, Geophys. Res. Lett. 8 (1981) 29–32.
[20] M.T. Zuber, D. Smith, F. Lemoine, G. Neumann, The shape and internal structure of the Moon from the Clementine mission, Science 266 (1994) 1839–1843.
[21] G.A. Neumann, M.T. Zuber, D.E. Smith, F.G. Lemoine, The lunar crust: global structure and signature of major basins, J. Geophys. Res. 101 (1996) 16.841–16.863.
[22] M.A. Wieczorek, R.J. Phillips, Potential anomalies on a sphere: applications to the thickness of the lunar crust, J. Geophys. Res. 103 (1998) 1715–1724.
[23] G. Latham, M. Ewing, J. Dorman, D. Lammlein, F. Press, N. Toksöz, G. Sutton, F. Duennebier, Y. Nakamura, Moonquakes, Science 174 (1971) 687–692.
[24] N. Mark, G. Sutton, Lunar shear velocity structure at Apollo sites 12, 14, and 15, J. Geophys. Res. 80 (1975) 4932–4938.
[25] Y. Nakamura, G.V. Latham, H.J. Dorman, Apollo lunar seismic experiment—final summary, J. Geophys. Res., Supplement, Proc. Lunar Planet. Sci. Conf. 13th, part 1, 87, 1982, pp. A117–A123.
[26] P. Lognonné, B. Mosser, Planetary seismology, Surv. Geophys. 14 (1993) 239–302.
[27] P. Lognonné, Planetary seismology, Annu. Rev. Earth Planet. Sci. 33 (2005) 19.1–19.34, doi:10.1146/annurev.earth.33.092203.122605.
[28] J. Gagnepain-Beyneix, P. Lognonné, H. Chenet, T. Spohn, D. Lombardi, Seismic models of the Moon and their constraints on the mantle temperature and mineralogy, Phys. Earth Planet. Inter. (submitted for publication).
[29] D.E. Smith, M.T. Zuber, G.A. Neumann, F.G. Lemoine, Topography of the Moon from Clementine lidar, J. Geophys. Res. 102 (1997) 1591–1611.
[30] M. Cooper, R.L. Kovach, J.S. Watkins, Lunar near-surface structure, Rev. Geophys. Space Phys. 12 (1974) 291–308.
[31] S. Sasaki, Y. Iijima, K. Tanaka, M. Kato, M. Hashimoto, H. Mizutani, Y. Takizawa, The SELENE mission: goals and status, Adv. Space Res. 31-11 (2003) 2335–2340.
[32] H. Mizutani, M. Osako, Elastic wave velocities and thermal diCusivities of Apollo 17 rocks and their geophysical implications, Proc. Lunar Sci. Conf., 4th ed., 1973, pp. 2891–2901.
[33] A. Tarantola, B. Valette, Inverse problems=quest for information, J. Geophys. 50 (1982) 159–170.
[34] K. Mosegaard, A. Tarantola, Monte Carlo sampling of solutions to inverse problems, J. Geophys. Res. 100 (1995) 12431–12447.
[35] M.A. Wieczorek, R.J. Phillips, The structure and compensation of the lunar crust, J. Geophys. Res. 102 (1997) 10933–10943.
[36] S.C. Solomon, J.W. Head, Lunar mascon basins: lava filling, tectonics, and evolution of the lithosphere, Rev. Geophys. Space Phys. 18 (1980) 107–141.
[37] A.S. Konopliv, S.W. Asmar, E. Carranza, W.L. Sjogren, D.N. Yuan, Recent gravity models as a result of the Lunar Prospector mission, Icarus 150 (2001) 1–18.
[38] M.A. Wieczorek and 15 coauthors, Constitution and structure of the lunar interior, in: B.J. Jolliff, M.A. Wieczorek (Eds.), New Views of the Moon, Rev. Min. Geochem., vol. 60, in press.
[39] W.H. Press, S.A. Teukolsky, W.T. Vetterling, B.P. Flannery, The Art of Scientific Computing, Cambridge Univ. Press, 1992.
[40] N. Goins, A. Dainty, N. Toksöz, Lunar seismology: the internal structure of the Moon, J. Geophys. Res. 86 (1981) 5061–5074.
[41] Y. Nakamura, Seismic velocity structure of the lunar mantle, J. Geophys. Res. 88 (B1) (1983) 677–686.
[42] A. Tarantola, Inverse Problem Theory, Elsevier, New York, 1987, 613 pp.
[43] N. Metropolis, S. Ulam, The Monte-Carlo method, J. Am. Stat. Assoc. 44 (1949) 335–341.